2017 American Control Conference
Sheraton Seattle Hotel
May 24–26, 2017, Seattle, USA

Enabling Demand Response Programs via Predictive Control of Building-to-Grid Systems Integrated with PV Panels and Energy Storage Systems

Meysam Razmara[◊], Guna R. Bharati[†], Drew Hanover[◊],
Mahdi Shahbakhti[◊], Sumit Paudyal[†], and Rush D. Robinett III[◊]

Abstract— **Demand Response (DR) program is one of the ancillary services to reduce the peak load contribution of buildings by altering the operation of dispatchable load including Heating, Cooling and Air-Conditioning (HVAC) load. In this paper, a Model Predictive Controller (MPC) is designed to optimize the power flows from the grid and Energy Storage Systems (ESS) to a commercial building equipped with HVAC systems and PV panels. The MPC framework uses the inherent thermal storage of the building and the ESS as a means to provide DR. Our results show that the proposed control framework for Building-to-Grid (B2G) systems can significantly reduce the maximum load ramp-rate of the electric grid to prevent duck-curve issues associated with increase in solar PV penetration into the grid. The B2G simulation testbed in this paper is based on the experimental data obtained from an office building, PV panels, and battery packs at Michigan Technological University integrated with a 3-phase distribution test feeder. Compared to the rule-based controller, the proposed predictive control approach can decrease the building operation electricity cost by 28% while decreasing maximum load ramp-rates by more than 70%.**

I. INTRODUCTION

Given the intermittent nature of renewable power generations and their increasing penetration into the power grid, electricity generation is altering from predictable and dispatchable to variable and non-dispatchable sources [1]. By increasing the portion of non-dispatchable power generation sources which often leads to a mismatch between power demand and generation due to weather events, an increase in the fluctuations of the electric grid power is leading to volatility of the electricity price in the market. As an example, customers in part of Pennsylvania -New Jersey- Maryland (PJM) experienced an 86-fold spike in electricity price due to extreme weather conditions in January 2014 [1], [2]. This issue inspires deployment of Demand Side Management (DSM) for adjusting power generation and load which is more critical by advent of Renewable Energy Sources (RES).

Ramp-rate is the rate that a generator increases generation (ramp-up) or decreases generation (ramp-down). Generators have different ramp-rate characteristics, e.g. coal-fired and nuclear facilities have very slow ramp-rates, compared to the fossil fuel-fired generators such as gas turbine generators. The fossil fuel generators or so-called 'peaker' power plants provide faster ramp-rates, and also faster start-up/shut-down. But this comes at the expense of higher operational costs and negative environmental impacts [3]. Peaks in demands cause undesirable spikes in electricity prices, transmission congestion, and, often requires to run inefficient and high Greenhouse Gas (GHG) emitting peaker power plants.

Large thermal storage capacity of buildings allows the HVAC system in buildings to act as an appropriate and flexible candidate to mitigate ramp-rate problems via Demand Response (DR) [4], [5]. DR refers to adjustment in power consumption of end-user customers (in our case buildings) in response to electricity price, incentives, or system reliability emergencies [6].

In the modern grid, DR becomes more important as volatility on the grid continues to increase [1], [3]. The DR provided by HVAC systems can make the electric grid more robust to intermittent renewable power generation. In [4], application of HVAC for DR in large power systems is discussed. The authors in [4] have compared control of fan speed, supply pressure/mass flow, thermostat set-points. Their results determine the trade-off between open-loop and closed-loop control for frequency regulation DR. Real-time pricing is studied as a method of DR in [7], [8].

As the DR programs become more prevalent, it is important to better understand the flexibility of a building integrated with Energy Storage Systems (ESS) and RES to provide DR for electric grid and utilities. This paper proposes a model predictive control framework for Building-to-Grid (B2G) systems which significantly reduces the maximum load ramp-rate of the power grid to prevent duck-curve issues [9] associated with increase in solar PV power penetration in the grid. The predictive controller uses B2G models including a building thermal model, PV model, battery model, and distribution grid model. In addition, weather prediction, a day-ahead Locational Marginal Pricing (LMP), irradiation prediction and occupancy of the building are fed to the MPC problem to calculate optimum operation of the demand flexibility. Our results show that compared to the rule-based controller, the proposed predictive control approach leads to 28% reduction in electricity cost of buildings while decreasing maximum ramp-rates by more than 70%.

This paper builds upon the B2G optimization framework in our previous studies [10]–[12]. The new contribution from this work includes (i) DR service by B2G optimization for load ramp-rate control of building loads, (ii) Modeling including experimental validation for PV panels, and (iii)

[◊] Meysam Razmara, Drew Hanover, Mahdi Shahbakhti and Rush D. Robinett III are with Mechanical Engineering-Engineering Mechanics Department of Michigan Technological University {mrazmara, djhanove, mahdish, rdrobine}@mtu.edu

[†]Guna R. Bharati, and Sumit Paudyal are with Electrical Engineering Department of Michigan Technological University {grbharati, sumitp}@mtu.edu

incorporating ESS and PV panels in a bidirectional B2G optimization framework.

II. B2G Configuration

Fig. 1 shows a proposed B2G topology schematic equipped with battery packs and PV panels. In this structure, the battery is responsible for mitigating the intermittent power generation from the PV panels and delivering the required power to the building to decrease the building operation cost and provide flexibility for DR programs required by grid. Building Energy Management System (BEMS) receives day-ahead electricity price from Market Operator (MO). In addition, weather and irradiation prediction which are now available online, are used in the predictive controller framework. In DR, a minimum impact on the occupants' comfort is desired; thus, lighting and appliences loads are considered non-dispatchable loads while heat-pump units or other HVAC systems are considered as the dispatchable loads in this topology.

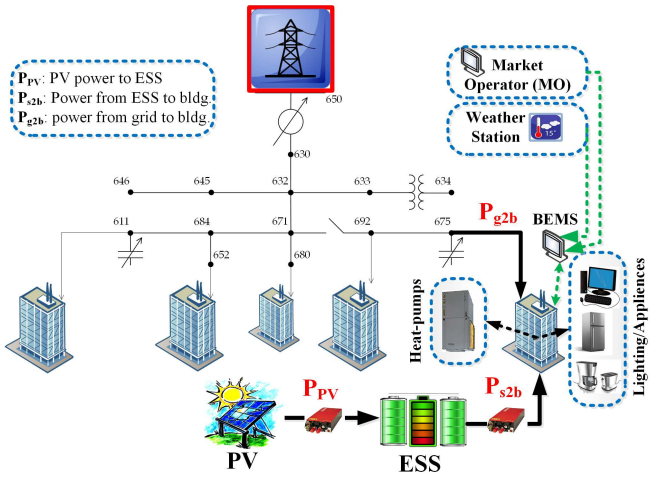

Fig. 1. Topology of the B2G system with ESS and solar power for the DR in this paper. The 3-phase distribution power system is connected to the buildings in nodes #611, #652, #680, #692, and #675.

In order to control the power consumption of the building and predict energy required by the building from grid, a mathematical model of building, battery, solar panels and inverters are required which is presented in Section III.

III. Mathematical Modeling

A. PV Panel Model

Solar arrays consist of solar cells that are connected in series and parallel depending upon the desired output power. Solar cells are semiconductor devices that convert solar radiation into electrical energy. An equivalent circuit for PV cells includes a series resistance, a current source in parallel with a diode, and a shunt or parallel resistance.

The output power of a solar panel is highly dependent on the irradiation level, temperature, and PV orientation. In order to predict power from a PV array, knowing the PV current-voltage relationship is necessary. In this study, we used a five-parameter model for a solar cell to calculate the current-voltage relationship from [13], [14]. In this model, the characteristics of the PV cell is described with a single diode [14]. The model incorporates the PV characteristic parameters including (i) short circuit current (I_{SC}), (ii) open circuit voltage (V_{OC}), (iii) maximum power point current (I_{MP}), (iv) maximum power point voltage (V_{MP}) and (v) temperature coefficient of V_{OC} and I_{SC} which are denoted with β_V, and α_I, respectively.

Eq. (1) presents the governing equation for a PV array that includes N_p parallel cells and N_s series cells. Eq. (1) shows an implicit relationship between voltage (V_{Ar}) and current (I_{Ar}) of an array [13], [14].

$$I_{Ar} = N_p I_L - N_p I_0 [exp(\frac{q(V_{Ar} + I_{Ar}\frac{N_s}{N_p}R_s)}{N_s n_I k T_c}) - 1] - \frac{V_{Ar} + I_{Ar}\frac{N_s}{N_p}R_s}{\frac{N_s}{N_p}R_p} \quad (1)$$

Where, I_L and I_0 denote photo current (i.e., light current), and diode saturation current, respectively. R_s and R_p are series and parallel resistance, respectively. n_I denotes the diode Ideality factor which is an index for recombination phenomena in the diode; q is the electron charge; k is the Boltzmann constant; T_c is the cell temperature.

Since measuring cell temperature is costly and the data is not available, the author in [15] proposed the method to calculate T_c as a function of the ambient temperature and the solar irradiation.

There are several methods to track Maximum Power Point (MPP) at different conditions. These methods are different in accuracy, convergence speed, and cost of electronic devices. In order to analytically find MPP voltage (V_{MP}) and current (I_{MP}) at any operating condition, the following equations set are solved simultaneously.

$$I_{MP} = N_p I_L - N_p I_0 [exp(\frac{q(V_{MP} + I_{MP}\frac{N_s}{N_p}R_s)}{N_s n_I k T_c}) - 1] - \frac{V_{MP} + I_{MP}\frac{N_s}{N_p}R_s}{\frac{N_s}{N_p}R_p} \quad (2a)$$

$$\frac{I_{MP}}{V_{MP}} = \frac{\frac{qN_pI_0}{N_s n_I k T_c} exp(\frac{q(V_{MP}+I_{MP}\frac{N_s}{N_p}R_s)}{N_s n_I k T_c}) + \frac{1}{\frac{N_s}{N_p}R_p}}{1 + \frac{qI_0R_s}{n_I k T_c} exp(\frac{q(V_{MP}+I_{MP}\frac{N_s}{N_p}R_s}{N_s n_I k T_c}) + \frac{R_s}{R_p}} \quad (2b)$$

In this study, we developed a mathematical model for 'BP SX3200B' solar panels. Detailed specifications of these solar panels are found in [16].

B. Battery Model

Based on Fig. 1, the battery packs act as the ESS component that are charged by PV panels and deliver power to the building while discharging. In this paper, a 65 kW LG Chem lithium-ion air-cooled battery pack with nominal capacity of 5 kWh is used. The battery model is based on the performance maps provided by the manufacturer [17].

Maximum charge and discharge power achievable by the battery at a given State of Charge (SOC) and temperature are determined based on the performance map.

The SOC of the battery is calculated using the following difference equation from [18].

$$SOC_{k+1} = SOC_k + \sum_{k}^{k+1} \frac{P_{PV_k} - P_{s2b_k}}{V_{B_k} C_B} \Delta t \tag{3}$$

Where P_{PV} is the power from PV panels which charges the battery packs; P_{s2b} is the power from the ESS to the building which is discharged from the battery packs; V_B is the voltage across the battery; C_B is the capacity of the battery. Validation of the battery model in this paper can be found in [18].

C. Building Model

In this study, a common thermal modeling approach known as the nodal approach [19] is used to model the heat transfer/generation of a building with electrical components such as capacitors, resistors, and current sources. Details of Resistance-Capacitance (RC) modeling for buildings can be found in our previous work [10]. The building model is validated using actual data from an office building at Michigan Technological University [19].

Building thermal model can be represented in state-space form by:

$$\begin{aligned} \dot{x}(t) &= f(x(t), u(t), w(t), t) \\ y(t) &= Cx(t) \end{aligned} \tag{4}$$

where, $x(t) \in \mathbb{R}^n$ is the state vector which includes buildings' room temperature. $y(t) \in \mathbb{R}^m$ is the output vector of the system that consists of thermal zones' temperature. The input vector includes the air mass flow rate and its temperature. C is the output matrix with proper dimension to return output, $y(t)$, from the system's states.

1) Building Predictive Controller: The main goal of optimal control on the building side is to minimize cost of electricity consumed by the building's HVAC system. For this purpose, HVAC power consumption, solar power generation, supplied power from battery packs, day-ahead forecast of weather and irradiation, and day-ahead time varying electricity price are taken into account. Building power consumption is characterized by [19]:

$$I_t^e = \sum_{t=1}^{24} P_t^{Bldg} \tag{5a}$$

$$P_{Bldg_t} = P_t^h + P_t^c + P_t^f + P_t^o \tag{5b}$$

where, I^e is the energy index. P_{Bldg} denotes the active power consumption of building. P^h, P^c, and P^f are heating, cooling and fan power, respectively. P^o includes lighting and appliances loads which are considered non-dispatchable load in this study. The HVAC load is considered dispatchable.

The objective function shown in Eq. (6a) is used to minimize energy cost of building's operation. In addition, soft constraints bounds (i.e., ϵ) for the room temperature are used to guarantee feasibility of optimal solution at all times. The following optimization problem is solved at each time step t, and the cumulative cost is calculated from t to t_{max}:

$$\min_{U_t, P_{s2b}, \overline{\epsilon}, \underline{\epsilon}} \{ (\sum_{t}^{t_{max}} \overbrace{(I_t^e - P_{s2b})}^{P_{g2b}} . \Omega^T) + \rho(|\overline{\epsilon}_t|_1 + |\underline{\epsilon}_t|_1) \} \tag{6a}$$

subject to:

$$x_{t+k+1|t} = Ax_{t+k|t} + Bu_{t+k|t} + Ed_{t+k|t} \tag{6b}$$

$$y_{t+k|t} = Cx_{t+k|t} \tag{6c}$$

$$SOC_{t+k+1|t} = SOC_{t+k|t} + \frac{\sum_{k}^{k+1} (P_{PV_{t+k|t}} - P_{s2b_{t+k|t}}) \Delta t}{V_{B_{t+k|t}} C_B} \tag{6d}$$

$$SOC_1 = SOC_{t_{max}} \tag{6e}$$

$$\underline{SOC} \leq SOC_{t+k+1|t} \leq \overline{SOC} \tag{6f}$$

$$0 \leq P_{PV_{t+k|t}} \leq f_{chg}(SOC, T_{amb}) \tag{6g}$$

$$0 \leq P_{s2b_{t+k|t}} \leq f_{dschg}(SOC, T_{amb}) \tag{6h}$$

$$\underline{\mathcal{U}}_{t+k|t} \leq u_{t+k|t} \leq \overline{\mathcal{U}} \tag{6i}$$

$$\underline{\Psi}_{t+k|t} \leq P_{g2b_{t+k+1|t}} - P_{g2b_{t+k|t}} \leq \overline{\Psi}_{t+k|t} \tag{6j}$$

$$P_{g2b_{k+t+1|t}} \leq \phi_{k+t+1|t} \tag{6k}$$

$$\underline{T}_{t+k|t} - \underline{\varepsilon}_{t+k|t} \leq y_{t+k|t} \leq \overline{T}_{t+k|t} + \overline{\varepsilon}_{t+k|t} \tag{6l}$$

$$\underline{\varepsilon}_{t+k|t}, \overline{\varepsilon}_{t+k|t} \geq 0 \tag{6m}$$

where P_{g2b} is the power flow of grid to the building. (6b) and (6c) constitute the building's state model. In (6b), d denotes disturbance matrix. (6d) denotes the battery pack model, (6e) shows the battery charge sustaining constraint that also helps to have a fair basis to compare different case studies in this paper. (6f) is the battery operation constraint defined by the battery manufacturer to reduce battery aging [20]. In this study, $\underline{SOC}$ and $\overline{SOC}$ are set to 30% and 70%, respectively. (6g) and (6h) are the charging and discharging rate limitation derived from the performance maps of the battery packs which are dependent on the temperature and SOC of the battery and T_{amb} (ambient temperature). (6i) is the constraint on the control input i.e., supply air temperature. (6j) is the ramp-rate constraint sent by utility or ISO in which $\underline{\Psi}_{t+k|t}$ and $\overline{\Psi}_{t+k|t}$ are load ramp-down rate and ramp-up rate limitations. (6k) denotes the constraint on the maximum feasible building load. The building receives $\underline{\Psi}_{t+k|t}$ and $\overline{\Psi}_{t+k|t}$ as DR signals from ISO.

Eq. (6l) is the output constraint on temperature of room and (6m) represents the constraint on slack variables. $U_t = [u_{t|t}, u_{t+1|t}, \cdots, u_{t+N-1|t}]$ represents control inputs vector and $u_{t+1|t}$ is the estimated value of u_{t+1} at time t; $\underline{\epsilon}_t = [\underline{\varepsilon}_{t+1|t}, \cdots, \underline{\varepsilon}_{t+N|t}]$ and $\overline{\epsilon}_t = [\overline{\varepsilon}_{t+1|t}, \cdots, \overline{\varepsilon}_{t+N|t}]$ are the slack variables. The slack variables' weight (ρ) in Eq. (6a) should be chosen large enough so the optimizer enforces the slack variables to take small values. Eq. (6l) defines the relationship between the room temperature and the slack variable value. Ω is LMP of electricity which is considered to be independent of power consumption by the building loads. $y_{t+k|t}$ is the vector of thermal zone temperature, $d_{t+k|t}$ is the disturbance load, and $\underline{T}_{t+k|t}$ and $\overline{T}_{t+k|t}$ for $k = 1, \cdots, N$

are the lower and upper bounds on the zone comfort level, respectively. $\underline{\mathcal{U}}_{t+k|t}$ and $\overline{\mathcal{U}}$ are the lower and upper limits on the supply air temperature delivered by the heat-pump of the HVAC system, respectively. The operational limit on the maximum supply air temperature is not time-varying; therefore, a time-invariant constraint $\overline{\mathcal{U}}$ is used.

D. Distribution Grid Optimization Model

Distribution Grid consists of series and shunt elements like cable/conductors, transformers, capacitor banks, regulators, loads, etc. We use a detailed distribution grid model from our previous work in [10]. In distribution optimization model, a coordination profile is generated considering maximization of building load penetration as an objective, which can be written as:

$$\text{Max}: \left\{ \sum_{m,p,t} \mathbb{R}\left(V_{m,p,t} \cdot \overline{I^{bl,max}_{m,p,t}}\right) \right\} \tag{7a}$$

subject to:

$$\begin{bmatrix} V_{i,p,t} \\ I_{se,j,p,t} \end{bmatrix} = \begin{bmatrix} A_{j,t} & B_{j,t} \\ C_{j,t} & D_{j,t} \end{bmatrix} \begin{bmatrix} V_{i+1,p,t} \\ I_{re,j,p,t} \end{bmatrix} \tag{7b}$$

$$I_{re,j-1,p,t} = I_{se,j,p,t} + I^{zl}_{i,p,t} + I^{cl}_{i,p,t} + I^{bl,max}_{i,p,t} \tag{7c}$$

$$V^{min}_m \leq |V_{m,p,t}| \leq V^{max}_m \tag{7d}$$

$$|I_{se,j,p,t}| \leq I^{max}_j \tag{7e}$$

$$|I_{re,j,p,t}| \leq I^{max}_j \tag{7f}$$

$$\sum_p \left| V_{itr,p,t}\, \overline{I_{se,tr,p,t}} \right| \leq ST_{tr} \tag{7g}$$

$$Ctap^{min} \leq Ctap_{t,p} \leq Ctap^{max} \tag{7h}$$

$$Ttap^{min} \leq Ttap_{t,p} \leq Ttap^{max} \tag{7i}$$

$$\phi_{m,p,t} = \mathbb{R}\left(V_{m,p,t} \cdot \overline{I^{bl,max}_{m,p,t}}\right) \tag{7j}$$

where, (7b), (7e) and (7e) are equality constraints of distribution optimization model and represent Kirchhoff's voltage and current laws, respectively. Similarly, (7d), (7e), (7f), and (7g) are inequality constraints and represent voltage limit, branch current limit, and transformer capacity limit in the distribution feeder. Eq. (7h) and (7i) represent tap position constraint in capacitor and transformer banks, where, $Ctap$ and $Ttap$ are capacitor and transformer tap positions, respectively. Eq. (7j) provides the upper bound on load for buildings needed in Eq. (6k).

In Eq. (7), p represents phase; i represents node; and j represents series element between nodes i and $i+1$. se and re indicate sending and receiving end, respectively. m represents the nodes in the feeder where buildings are connected. I and V are complex current and voltage vectors in a feeder. Superscripts zl, cl, and bl represent constant impedance, current, and building loads.

IV. Simulation Results

The building, battery packs and PV panel models are implemented in MATLAB®. YALMIP Toolbox [21] in MATLAB is used to provide a symbolic syntax to formulate the optimization problem and interfaces with the solver. The distribution grid optimization model is developed in GAMS [22].

Weather forecast, irradiation, and LMP data are the inputs required for the B2G optimization models. For LMP, we use the data from Midcontinent Independent System Operator (MISO) [23]. Room air temperature bounds are set based on ANSI/ASHRAE Standard 55-2013.

The nodal results shown in this section, are presented for the building at node #675. System level ramp-rates, and load factors are calculated for the 3-phase distribution grid model. For MPC simulation, a prediction horizon of $N = 12$ is used with time step of $\Delta t = 30$ minutes. Here, we compare building unidirectional MPC, and B2G MPC with conventional rule-based control (RBC).

A. Unoptimized Rule Based Control (RBC)

In rule-based control of buildings, when temperature goes beyond a dead-band, the HVAC RBC keeps the heat-pump compressor ON for the duration of Δt. In the next time step, the RBC checks the room temperature and SOC again and determines whether the room temperature is within the comfort bounds to determine power dispatch of battery packs.

Table I shows the commercial building running cost which includes HVAC, lighting, and appliances and also nodal load factor (LF). Load factor is the ratio of average power to peak power and defines how efficient power infrastructure is being utilized.

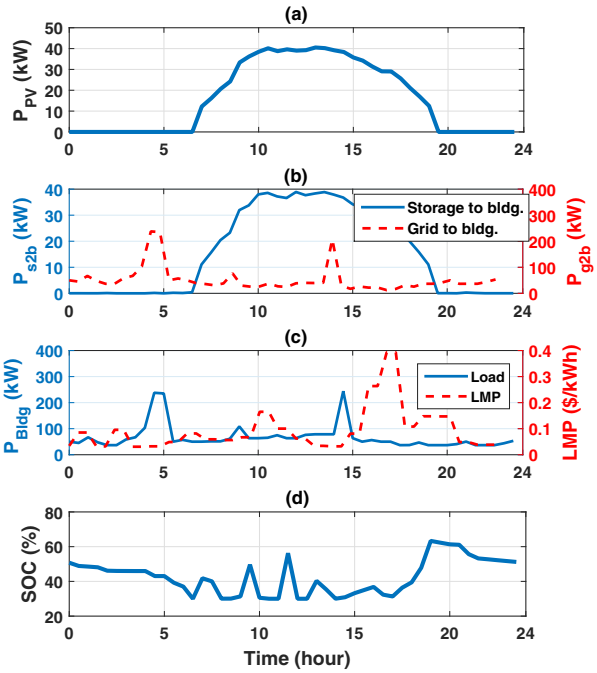

Fig. 2. Power flow of the building connected to node #675 under Unidirectional control. (a) power generated by the solar panels, (b) power from the ESS to the building (P_{s2b}), and power consumed in the building delivered by the grid, (c) power consumption by the building and the LMP, and (d) SOC of the battery packs in the building.

TABLE I

PERFORMANCE COMPARISON OF THREE DIFFERENT BUILDING/GRID CONTROL TECHNIQUES.

Optimization Type	Monthly Bldg. elec. cost [$]	System max ramp-up $[GW/h]$	System max ramp-down $[GW/h]$	Node #675 load factor [-]	System load factor [-]	Bldg. cost saving* [%]
Unoptimized	3571	1.573	1.377	0.67	0.704	0
Unidirectional	2463	0.911	1.103	0.69	0.793	31
Bidirectional	2588	0.277	0.365	0.82	0.855	28

*Saving percentage is calculated by $\frac{x-x_0}{x_0} \times 100$, where x_0 is the electricity cost for the 'Unoptimized' RBC case.

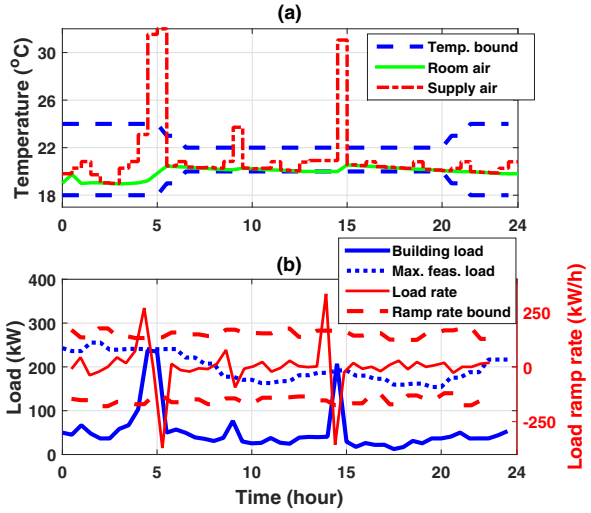

Fig. 3. Building Unidirectional control: (a) Control input and resulting room air temperature profile for the unidirectional controller, (b) Building electricity load versus maximum feasible load for node #675; Load rate versus ramp-rate bound (ramp-up and ramp-down limits).

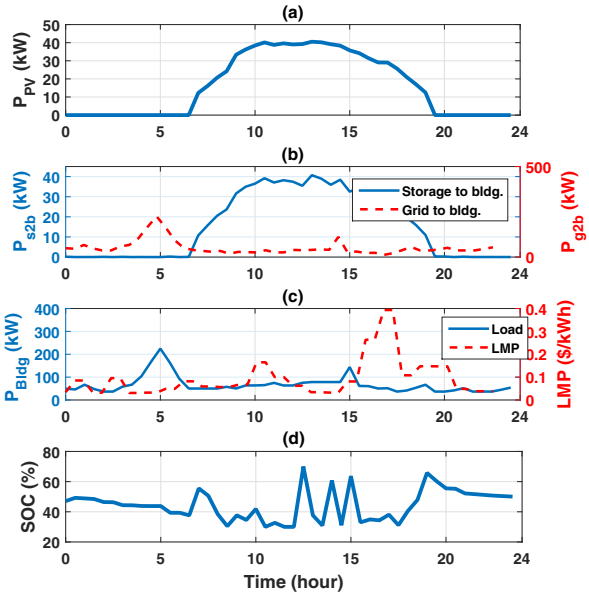

Fig. 4. Power flow of the building connected to node #675 under Bidirectional control. (a) power generated by the solar panels, (b) power from the ESS to the building (P_{s2b}), and power consumed in the building delivered by the grid, (c) power consumption by the building and the LMP, and (d) SOC of the battery packs in the building.

B. Unidirectional Predictive Control

In this section, the results are presented for uncoordinated demand and grid side optimization; thus, the term 'Unidirectional' is used.

Fig. 2 illustrates different power flows from energy sources to the building. Fig. 2 (a) shows non-dispatchable PV power into the ESS. Fig. 2 (b) represents two power flows to the building, P_{s2b} and P_{g2b}. The building cost optimizer minimizes operation cost by adjusting the optimal values of P_{s2b} and P_{g2b} at each time step. Fig. 2 (c) illustrates the building total load and LMP. As seen in Fig. 2 (c), the building peak load occurs when LMP has lower values. SOC of the ESS is shown in Fig. 2 (d), showing SOC of the battery packs is maintained at 50% at the end of the day. This helps to have a fair basis to compare different case studies in this paper. Fig. 3 shows the results of unidirectional MPC for the B2G system. Fig. 3 (a) depicts the building air temperature along with temperature bounds and the MPC control inputs (i.e., supply air temperature). Fig. 3 (b) shows the building load (P_{g2b}), and the maximum feasible load for buildings at node #675. In addition, the rate of P_{g2b} and the load ramp limits are shown in Fig. 3 (b). The building predictive controller tries to minimize the operation cost by utilizing power from ESS (P_{s2b}) and power from grid (P_{g2b}) when the electricity price is low. However, the building controller does not consider the grid limitation, as seen by the violation in Fig. 3 (b) at 4:30 AM and 2:30 PM. Ramp-up and ramp-down limitations ($\overline{\Psi}$, and $\underline{\Psi}$) are determined by ISO or utility.

The building and grid side operation results are summarized in Table I. The results show 31% reduction in the building electricity cost and also an average of 30% reduction in the distribution system ramp-up/down compared to the unoptimized case.

C. B2G Bidirectional Predictive Controller

In this section, we consider the bilevel DR information exchange between buildings and grid as discussed in details in [10]. Maximum feasible load, ramp-up and ramp-down limitation, and LMP are sent to the building as DR signals in a day-ahead or real-time fashion. The BEMS uses the DR signal as the constraints of the MPC problem and solves the optimization problem to provide DR services and minimize the building electricity cost. All other constraints are the same as those in the unidirectional predictive controller.

Fig. 4 shows power flows in the building under the bidirectional predictive controller. Fig. 5 shows the resulting building air temperature and constraints. Fig. 5 (b) shows the building load and rate of the building load under the bidirectional control framework. As seen in Fig. 5 (b), unlike the unidirectional controller, the B2G predictive controller meets the ramp-rate DR signal and does not exceed the maximum feasible load constraints, Eq. (6j) and Eq. (6k).

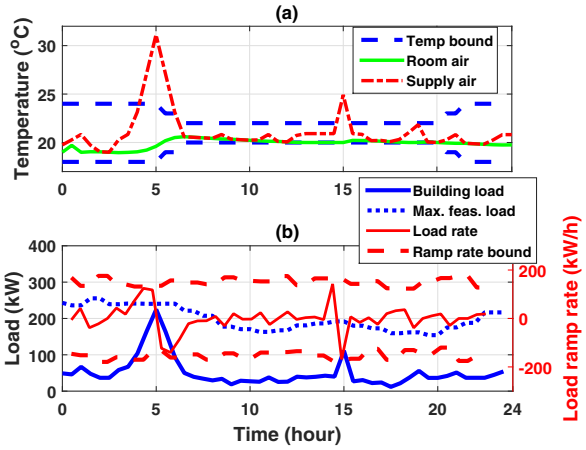

Fig. 5. Building Bidirectional control: (a) control input and resulting room air temperature profile for the bidirectional controller, (b) building electricity load versus maximum feasible load for node #675; Load rate versus ramp rate bounds (ramp-up and ramp-down limits).

D. Controller Comparison

The monthly building energy cost is listed in TABLE I. Compared to the RBC, unidirectional control framework leads to 31% cost saving and 41% and 20% less maximum ramp-up and ramp-down, respectively. Bidirectional control results in 28% less electricity cost, compared to RBC.

The key takeaway from this comparison is that bidirectional MPC drops the maximum ramp-up and ramp-down by 82% and 73%, respectively. This decrease is at the expense of few percent more electricity cost. However, the benefits that the power grid achieves from DR could be very significant.

V. Discussion and Conclusion

This paper introduces a predictive bidirectional control framework for B2G systems to decrease the building operational cost and to provide DR flexibility for the electric grid. DR programs can stabilize grid system by mitigating both generation fluctuation and high ramp-rates issues. An experimentally validated PV model, battery packs as the ESS, an experimentally validated building thermal model and a mathematical model for the 3-phase distribution grid were integrated to create the B2G modeling framework.

For the case studies in this paper, the proposed predictive control of B2G system could reduce commercial buildings monthly electricity costs by 28%, compared to the unoptimized rule-based control while adjusting load ramp-rates. By decreasing load ramp-rates the need for costly GHG-emitting fast ramp-rate generators decreases and also stabilizes the electric grid by mitigating intermittent solar power generation.

Acknowledgment

This work was supported in part by the US National Science Foundation (Grant #1541148) and the Richard and Elizabeth Henes Professorship of Mechanical Engineering at Michigan Technological University. Authors would like to acknowledge Keweenaw Research Center (KRC) at Michigan Technological University for providing the experimental power data of PV panels for this paper. In addition, LG Chem Power Inc. is gratefully appreciated for providing the battery packs in this study.

References

[1] M. Behl, F. Smarra, and R. Mangharam. "DR-Advisor: A data-driven demand response recommender system". *Applied Energy*.

[2] PJM Interconnection LLC (PJM). "PJM response to consumer reports on 2014 winter pricing".

[3] US DOE SOLAR ENERGY TECHNOLOGIES PROGRAM. The Importance of Flexible Electricity Supply. Solar Integration Series 1 of 3 (Accessed on 04-14-2016).

[4] I. Beil, I. Hiskens, and S. Backhaus. Frequency Regulation From Commercial Building HVAC Demand Response. *Proceedings of the IEEE*, 104(4):745–757, 2016.

[5] M. Maasoumy, B.M. Sanandaji, A. Sangiovanni-Vincentelli, and K. Poolla. Model Predictive Control of Regulation Services from Commercial Buildings to the Smart Grid. In *American Control Conference (ACC)*, pages 2226–2233. IEEE, 2014.

[6] Benefits of Demand Response in Electricity Markets and Recommendations for Achieving Them. *US Department of Energy (DOE), Technical Report to the United States Congress*, 2006.

[7] R. Sioshansi and W. Short. Evaluating the Impacts of Real-time Pricing on the Usage of Wind Generation. *IEEE Transactions on Power Systems*, 24(2):516–524, 2009.

[8] H. Allcott. Rethinking Real-time Electricity Pricing. *Resource and Energy Economics*, 33(4):820–842, 2011.

[9] P. Denholm, M. O'Connell, G. Brinkman, and J. Jorgenson. Overgeneration from Solar Energy in California: A Field Guide to the Duck Chart. *National Renewable Energy Laboratory, Tech. Rep. NREL/TP-6A20-65023, Nov*, 2015.

[10] M. Razmara, G. R. Bharati, M. Shahbakhti, S. Paudyal, and R. D. Robinett III. Bilevel Optimization Framework for Smart Building-to-Grid Systems. *IEEE Trans. on Smart Grid*, (99), 2016.

[11] M. Razmara, G.R. Bharati, M. Shahbakhti, S. Paudyal, and R.D. Robinett. Bidirectional Optimal Operation of Smart Building-to-Grid Systems. In *American Control Conf. (ACC)*, pages 288–293, 2015.

[12] G. R. Bharati, M. Razmara, S. Paudyal, M. Shahbakhti, and R.D. Robinett III. "Hierarchical Optimization Framework for Demand Dispatch in Building-Grid Systems". In *PES GM*, 2016.

[13] W. De Soto, S.A. Klein, and W.A. Beckman. Improvement and Validation of a Model for Photovoltaic Array Performance. *Solar energy*, 80(1):78–88, 2006.

[14] H. Tian, F. Mancilla-David, K. Ellis, E. Muljadi, and P. Jenkins. A Cell-to-Module-to-Array Detailed Model for Photovoltaic Panels. *Solar Energy*, 86(9):2695–2706, 2012.

[15] G.M. Masters. *Renewable and Efficient Electric Power Systems*. John Wiley & Sons, Chapter 5, 2013.

[16] BP solar. BP SX3200B (200W) Solar Panel, (Accessed on Aug. 8^{th}, 2016), *http://www.solardesigntool.com/components/module-panel-solar/BP/9/ SX3200B/specification-data-sheet.html/*.

[17] LG Chem Power Inc. *5kWh Air Cooled Technical Manual*. 2013.

[18] A. Solouk, M. Shakiba-herfeh, K. Kannan, H. Solmaz, P. Dice, M. Bidarvatan, N.N.T. Kondipati, and M. Shahbakhti. Fuel Economy Benefits of Integrating a Multi-Mode Low Temperature Combustion (LTC) Engine in a Series Extended Range Electric Powertrain. Technical report, SAE Technical Paper, 2016-01-2361, 2016.

[19] M. Maasoumy, M. Razmara, M. Shahbakhti, and A. Sangiovanni Vincentelli. Handling model uncertainty in model predictive control for energy efficient buildings. *J. of Energy and Buildings*, 77, 2014.

[20] M. Jafari, A. Gauchia, K. Zhang, and L. Gauchia. Simulation and Analysis of the Effect of Real-World Driving Styles in an EV Battery Performance and Aging. *IEEE Transactions on Transportation Electrification*, 1(4):391–401, 2015.

[21] J. Löfberg. YALMIP: A toolbox for modeling and optimization in MATLAB. In *IEEE International Symposium on Computer Aided Control Systems Design*, pages 284–289, 2004.

[22] GAMS Development Corporation. (2014, Dec 10). *General Algebric Modeling System, Release 24.2.1*.

[23] MISO. (2014, Sep 3). Midcontinent Independent System Operator.